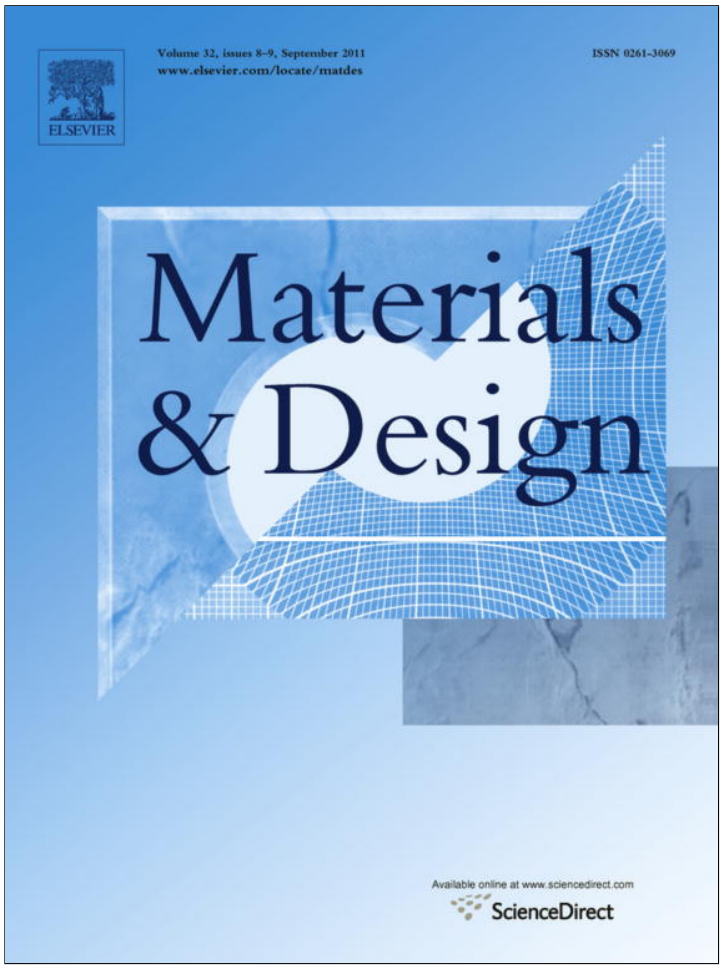

Materials and Design 32 (2011) 4580–4585

Contents lists available at ScienceDirect

Materials and Design

journal homepage: www.elsevier.com/locate/matdes

Short Communication

Modeling of microstructure and mechanical behavior of ultra fine grained aluminum produced by accumulative roll-bonding

A. Rezaee-Bazzaz *, S. Ahmadian, H. Reihani

Department of Metallurgy and Materials Engineering, Faculty of Engineering, Ferdowsi University of Mashhad, Mashhad, Iran

ARTICLE INFO

Article history:
Received 3 February 2011
Accepted 5 April 2011
Available online 20 April 2011

ABSTRACT

Mechanical behavior of AA1100 aluminum alloy processed by accumulative roll-bonding was modeled on the basis of a generalized three-dimensional dislocation-density-based two-phase composite model. The simulated yield stress and cell size were compared with the experimental data, obtained by accumulative roll-bonding after several passes. A good agreement between experimental and simulated results was obtained. The results showed that both yield stress and average cell size of the ultra fine grained materials, produced by accumulative roll-bonding, can be simulated using a dislocation-density-based two-phase model. Moreover, dynamic recovery in cell interior was governed by cross slip, while climb processes were responsible for that in cell walls.

1. Introduction

Severe plastic deformation (SPD) processing has been widely used for producing bulk ultra fine grained materials, having grain sizes in the sub-micrometer or nanometer range [1–3]. Several SPD processing techniques, such as accumulative roll-bonding (ARB) [4], cyclic extrusion and compression (CEC) [5], multi-directional forging (MDF) [6], equal channel angular pressing (ECAP) [7], and high pressure torsion (HPT) [8] have been developed and successfully utilized for producing sub-micron materials. Among these SPD techniques, ARB has unique characteristics. This process can be performed by the conventional rolling mills, and thus, it is capable of producing ultra fine grain sheets in a mass production scale with low price [4]. Accumulative roll-bonding involves securely stacking two sheets of the same materials after proper surface treatments. These treatments, may involve degreasing and surface contaminant removal with the use of steel wire brush. After surface treatment, the stacked sheets are usually preheated and rolled to a reduction of 50%. The rolled sheet is cut into two equal halves and this sequence is repeated as many times as necessary [4,9,10].

Grain refinement by severe plastic deformation is often related to the evolution of subgrain or dislocation cell boundaries [11], although the mechanisms of grain refinement are not fully understood. Tsuji et al. reported that the formation process of ultra fine grains in ARB is a continuous recrystallization phenomenon characterized by grain subdivision, recovery and even short range grain boundary migration to form ultra fine grains or subgrains [9]. Lee et al. have found that shear strain plays a decisive role in forming ultra fine grains during accumulative roll-bonding [12]. Based on the studies of Saito et al. [4], high shear strains are produced in the specimen surface because of the friction between roll and the specimen surface. This shear strain increases the imposed strain and promotes grain refinement. Moreover, in ARB process the surface layers shift inside the specimen by repeating each pass. Therefore, the shear strains affect the whole thickness of the specimen and make a complicated shear strain distribution which may assist grain refinement.

Estrin et al. [13] proposed a two-dimensional dislocation cell structure model which has been recently generalized to three-dimensional states [14]. The model takes into account strain rate sensitivity and evolution of cell structure [15] and can predict the strain hardening of dislocation cell-forming materials during all stages of hardening; from stage II up to the end of stage V. There have been several attempts to predict stress–strain behavior and microstructure produced by some SPD processes by the use of the dislocation cell structure model. McKenzie et al. [16] predicted the behavior of a wrought AA6016 alloy during ECAP up to 16 passes using a two-phase composite model, and showed that the model can predict the evolution of cell wall and cell interior dislocation densities very well. They also found that these parameters are functions of accumulated plastic strain as well as the level of hydrostatic pressure. Hosseini and Kazeminezhad [17–19] utilized the dislocation-density-based model for simulating the ECAP process and found that using this model, different microstructures produced by ECAP with different die shapes can be predicted fairly well. They also investigated deformation behavior of Cu, Al and Ta through ECAP and showed that the dislocation-density-based model can simulate the behavior of these materials well. The dislocation-density-based model has also been applied to the case of HPT, where a good correlation between simulated and

* Corresponding author. Tel.: +98 5118763305.
E-mail address: bazaz-r@um.ac.ir (A. Rezaee-Bazzaz).

0261-3069/$ - see front matter © 2011 Elsevier Ltd. All rights reserved.
doi:10.1016/j.matdes.2011.04.011

experimental microstructures was obtained [20]. It was claimed that a controversial issue of occurrence of uniform microstructure as a result of an inherently nonuniform process was resolved.

The short review presented here, shows that although the dislocation-density-based model has been used for modeling ECAP and HPT, there has been no attempt to simulate the ARB process using this approach. Since the main mechanisms of grain refinement in different SPD processes are almost the same, application of dislocation-density-based model for simulating ARB process seems to be rational. The aim of this work is thus to show whether or not dislocation-density-based model can be used for simulating yield stress and microstructure produced by ARB of AA1100 aluminum alloy.

2. Model description

A three-dimensional version of the dislocation-density-based strain hardening model [13,14], which has been used in this study, is briefly reviewed for the sake of completeness. In this model, it is assumed that the material consists of two distinct but not independent phases; cell walls with dislocation density of ρ_w and cell interiors containing dislocations with lower density of ρ_i. The total dislocation density ρ_t is obtained by rule of mixtures:

$$\rho_t = f\rho_w + (1-f)\rho_i \tag{1}$$

where f is the volume fraction of cell walls. It has been reported that f decreases with strain, monotonically [21] and its evolution can be described by the following empirical equation [13]:

$$\frac{f-f_\infty}{f_0-f_\infty} = \exp\left(-\frac{\gamma^r}{\Omega}\right) \tag{2}$$

In the above equation f_0 is the initial value of f, f_∞ refers to the saturation value of f at large strains and Ω shows the rate of variation of f with respect to shear strain, γ^r.

The average cell size, d, is inversely related to total dislocation density by

$$d = \frac{K}{\sqrt{\rho_t}} \tag{3}$$

where K is the cell size factor and decreases by increasing the accumulated shear strain, similar to cell wall volume fraction variation:

$$\frac{K-K_\infty}{K_0-K_\infty} = \exp\left(-\frac{\gamma^r}{\Gamma}\right) \tag{4}$$

where K_0, K_∞ and Γ are numerical constants.

The evolution of the dislocation density in cell interiors and cell walls is governed by the following equations, respectively [13].

$$\dot{\rho}_i = \frac{\alpha^*}{\sqrt{3}}\frac{\sqrt{\rho_w}}{b}\dot{\gamma}_w - \frac{6\beta^*\dot{\gamma}_i}{bd(1-f)^{1/3}} - R_i\left(\frac{\dot{\gamma}_i}{\dot{\gamma}_0}\right)^{-1/n_i}\dot{\gamma}_i\rho_i \tag{5}$$

$$\dot{\rho}_w = \frac{6\beta^*\dot{\gamma}_i(1-f)^{2/3}}{bdf} + \frac{\sqrt{3}\beta^*\dot{\gamma}_i(1-f)\sqrt{\rho_w}}{fb} - R_w\left(\frac{\dot{\gamma}_w}{\dot{\gamma}_0}\right)^{-1/n_w}\dot{\gamma}_w\rho_w \tag{6}$$

The first term in the right hand side of Eq. (5) shows the rate of dislocation generation in cell interiors by the Frank-Read mechanism. The second term represents the loss rate of cell interior dislocations by moving into the walls and becoming part of wall structure and the last term describes the annihilation rate of dislocations in the cell interior by dynamic recovery. The geometry parameters, α^* and β^* are considered to be constants, and R_i, n_i, $\dot{\gamma}_i$, $\dot{\gamma}_w$ and $\dot{\gamma}_0$ are the recovery factor in the cell interior, recovery exponent in the cell interior, shear strain rate in the cell interior, shear strain rate in cell walls and reference shear strain rate, respectively. The first term in the right hand side of Eq. (6) represents the dislocation density gain in the walls caused by the loss of dislocations in cell interiors. The second term expresses the increase of dislocation densities in the walls by activation of the Frank-Read sources at the interface by dislocations coming from cell interiors, and the third term accounts for the annihilation of cell wall dislocations by dynamic recovery at high strains. R_w and n_w are the recovery factor and recovery exponent in cell walls, respectively. To satisfy strain compatibility along the interface between cell interiors and cell walls, the following relation is imposed [14]:

$$\dot{\gamma}_i = \dot{\gamma}_w = \dot{\gamma}^r \tag{7}$$

Solving Eqs. (5) and (6) simultaneously by numerical methods, dislocation densities in both cell interiors and cell walls are computed. Using Eq. (1), the total dislocation density can also be calculated. The yield stress of the studied polycrystalline material is obtained based on the following equation:

$$\sigma_y = \sigma_0 + \alpha MGb\sqrt{\rho_t} \tag{8}$$

where σ_0 is the lattice friction stress at a constant temperature, G is the shear modulus, α is a numerical constant, and M is the Taylor factor. The present model is also able to predict the average cell size of the material by using Eq. (3).

3. Experimental

3.1. Material and processing

The material used was 1 mm thick commercially pure aluminum (AA1100) sheet, the chemical composition of which is shown in Table 1. From this sheet, samples with dimensions 200 mm × 30 mm × 1 mm were cut and used for the subsequent processing. The specimens were fully annealed at 673 K for 1 h to eliminate any effect of previous thermomechanical history. Standard metallographic procedures revealed that the mean grain size of the specimens after annealing was about 33 μm.

Two specimens prepared in the manner mentioned above were ARB processed. To achieve proper bonding between the specimens, their surfaces were wire brushed and degreased by acetone, before two samples were securely stacked by steel wires at the corners of the assembled specimens. The assembly was preheated to 453 K for 5 min and then rolled to 50% reduction without lubrication. The roll diameter was 180 mm and the peripheral speed was 22.7 m min^{-1}. The produced sheet was cut into two equal halves, and surface treatments, stacking, preheating and rolling stages were repeated up to 8 passes ($\varepsilon = 6.4$). The principles of the ARB process are schematically illustrated in Fig. 1. The 50% reduction at 453 K was quite enough to bond the sheets and no fracture at bonded boundaries was observed during the experiment. Based on the roll diameter and its peripheral speed, the mean equivalent strain rate of the ARB process was 44.5 s^{-1}.

3.2. Mechanical testing

Tensile specimens, 50 mm long and 12.5 mm wide, were machined from the ARB processed sheets. Tensile direction was parallel to the rolling direction. Tensile tests were carried out at ambient temperature using a screw driven Zwick Z250 universal testing

Table 1
Chemical composition of the AA1100 aluminum alloy.

Al	Si	Fe	Cu	Mn	Mg	Zn	Ti	Ni	Ca
Bal.	0.171	0.345	0.055	0.009	0.006	0.025	0.005	0.002	0.011

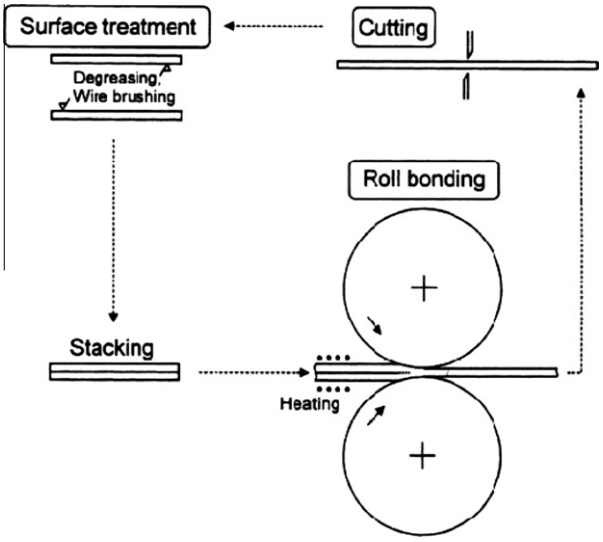

Fig. 1. Schematic illustration of the ARB process [4].

machine at a constant cross head speed of 6 mm min^{-1}, corresponding to an initial strain rate of 2×10^{-3} s^{-1} .

Microhardness of the ARB processed specimens was measured by a Buhler microhardness testing machine using the Vickers indenter under applied load of 25 g. Each reported hardness was an average of at least five separate measurements taken at random places on the surface of the ARB processed sheet. All the indentations were at least 5 mm away from the edges and from other indentations.

3.3. TEM observations

The microstructural observation by transmission electron microscopy (TEM) was done for the specimens after ARB. To prepare TEM thin foils parallel to the rolling direction, specimens were ground to a thickness of about 100 μm and then twin-jet electropolished using a 33% HNO_3 and 66% CH_3OH solution at −30 °C and 20 V. Leo 912 transmission electron microscope operated at 120 kV was used for microstructural examination.

4. Results and discussion

Fig. 2 shows the optical micrograph of (RD–ND) sections of the ARB processed sheets after different passes. As it is clear from the figure, proper bonding occurred between the layers and except the last interface which is partially observable, other regions are properly bonded. It is note worthy that although some edge cracks appeared during rolling after several passes; satisfactory sheets were obtained in most cases even after 8 passes of ARB.

Fig. 3a and b shows the respective variations of yield stress and microhardness with respect to ARB passes. According to Fig. 3a, the yield strength of the studied material increases with increasing the imposed strain. The maximum strength gain occurs after the first pass of ARB. Yield stress of the roll-bonded material changes from 58 MPa at the start of the process to 215 MPa after 8 passes. This is approximately 3.7 times greater than the yield stress of the material at the start of the process. Similar changes in yield strength have been already reported for the same material processed by the same method [22]. According to Fig. 3b, the trend of microhardness changes of the studied material with respect to ARB passes is the same as the trend of yield strength changes with ARB cycles. This fact shows that there exist a correlation between yield stress and microhardness in the ARB processed materials similar to those usually observed in the conventionally processed materials.

As mentioned earlier, in the dislocation-density-based model, the material is assumed to be composed of cell interiors and cell walls. According to the published reports, aluminum is a dislocation cell-forming material and the size of the dislocation cells depends on the dislocation density [17,22–24]. All of the model parameters and constants which are necessary for application of this model to ARB process of aluminum are summarized in Table 2. It is worth noting that, the parameters quoted in Table 2

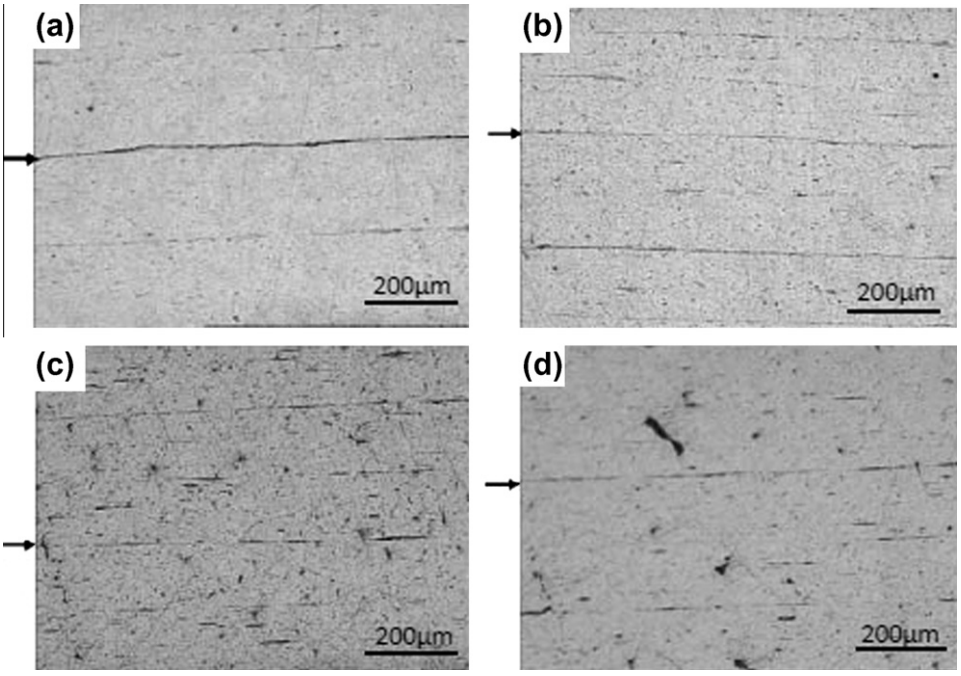

Fig. 2. Optical micrographs of (RD–ND) sections of the commercially pure aluminum after ARB: (a) one, (b) two, (c) four and (d) eight cycles (last interfaces indicated by arrows).

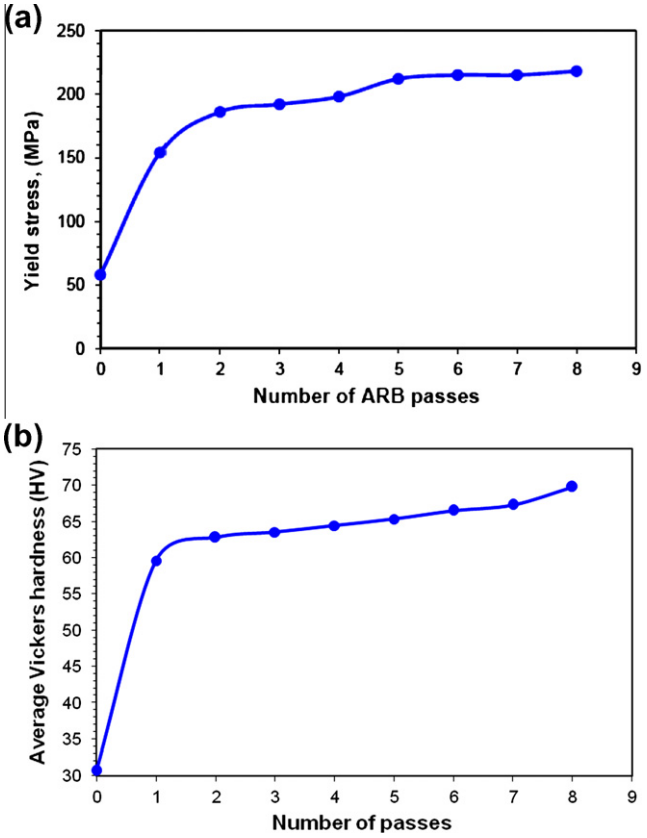

Fig. 3. (a) Variations of yield stress and (b) microhardness with number of ARB passes.

Table 2
The values of parameters and constants used in the model [16–19].

α^*	0.0024
β^*	0.0054
K_i	13
K_∞	6.5
α	0.25
M	3.06
G (MPa)	26.3×10^3
f_0	0.25
f_∞	0.06
Ω	2.11
$\dot{\gamma}_0^r$ (s^{-1})	1
$\rho_i^{t=0}$ (m^{-2})	10^{13}
$\rho_w^{t=0}$ (m^{-2})	10^{14}
Γ	3.85
R_i	11.5
R_w	6.9
n_i	67
n_w	4
b (m)	2.86×10^{10}

have been obtained for deformation of aluminum at room temperature but in this study, deformation was carried out at 423 K. Careful temperature measurement of the deforming sheets showed that the temperature of the sheet during deformation is 423 K which is about 30 K less than preheating temperature of the sheet. Therefore, the recovery exponent of the cell interiors, n_i, and the recovery factor of the cell walls, R_w, should be modified according to the deformation temperature. It has been reported that recovery factor and recovery exponent of the cell interiors are independent

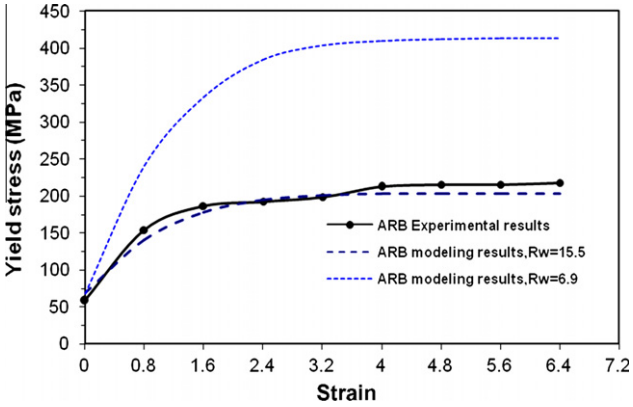

Fig. 4. Variation of yield stress with accumulated strain.

of temperature and inversely proportional to the absolute temperature, respectively [20,25]. Therefore, the value of n_i at 423 K should be modified based on the following equation:

$$\frac{n_i^{298}}{n_i^{423}} = \frac{423}{298} \tag{9}$$

There are two possibilities for recovery mechanism in cell walls; cross slip and edge dislocation climb [20,25]. The value of recovery factor in cell walls, R_w, is temperature independent in the case of cross slip. Hence, the value which is assigned to R_w is the same as that mentioned in Table 2 when the recovery mechanism of the cell walls assumed to be cross slip. The temperature dependence of R_w in the case of edge dislocation climb is assumed to be described by

$$R_w^T = \exp\left(-\frac{A}{T}\right) \tag{10}$$

Therefore, the value of R_w is modified based on Eq. (10), when the recovery mechanism of cell walls is assumed to be edge dislocation climb. The calculated value of n_i at 423 K is 47.2 and the computed value for R_w is 15.5 when the recovery mechanism of cell walls is edge dislocation climb.

The results of dislocation-density-based model for predicting the variation of yield stress with accumulated strain, assuming either of the recovery mechanisms in cell walls are illustrated in Fig. 4. For comparing the predicted results with experimentally determined yield stresses, the yield stress variation with accumulated strain obtained by experiment was superimposed on Fig. 4. It is clear from this figure that the assumption of cross slip as the recovery mechanism of cell walls leads to a severe increase in yield strength and does not correlate with experimental results, while considering edge dislocation climb as the recovery process in the cell walls produces predications for variation of yield stress with accumulated strain, which agree well with experimental results. Thus, it can be suggested that in the material processed by ARB, cross slip is the recovery process for the cell interiors and edge dislocation climb is responsible for recovery in cell walls.

Fig. 5a and b shows the TEM microstructure of the studied material after 8 passes of ARB together with the corresponding selected area diffraction pattern, respectively. It is clear that ultra fine grains are produced in the material after 8 passes of ARB. The mean grain size of the material was measured using linear intercept method and it was found that eight cycles of ARB produces the ultra fine grain material with grain sizes in the range of 300–450 nm. The ring pattern of SAD is an evidence for the existence of fine grains with high angle boundaries. Such a microstructure is similar to that reported for the same material processed by the same method [23,24].

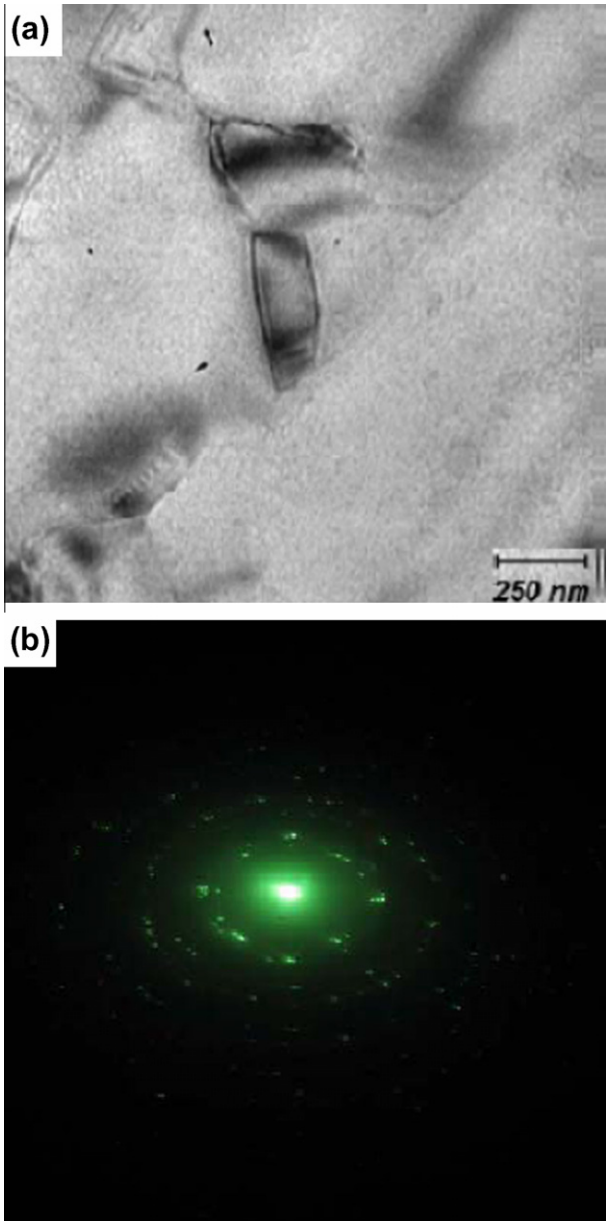

Fig. 5. TEM micrographs and the corresponding SAD pattern of commercially pure aluminum after 8 passes of ARB.

In the application of the model to the ARB process in the present study, it is tacitly assumed that a new refined grain structure emerges as the misorientation between cell structure increases with strain. The cell structure can thus be considered as grain structure, similar to the assumptions made in application of the model to ECAP and HPT [16,20,25]. Therefore, in this modeling approach, the theoretically calculated average cell size is assumed to be the average grain size which calculated by the model and can be compared with the experimentally determined average grain size. Changes of the cell size as a function of accumulated strain predicted by the dislocation-density-based model together with experimentally determined average cell size changes by accumulated strain obtained in this study and reported in the literature were shown in Fig. 6. As the figure shows, the maximum decrease in the average cell size occurs after the first pass of ARB and there is a good agreement between experimental and predicted results, though some experimental data were obtained from other studies in which the experimental parameters were not necessarily similar

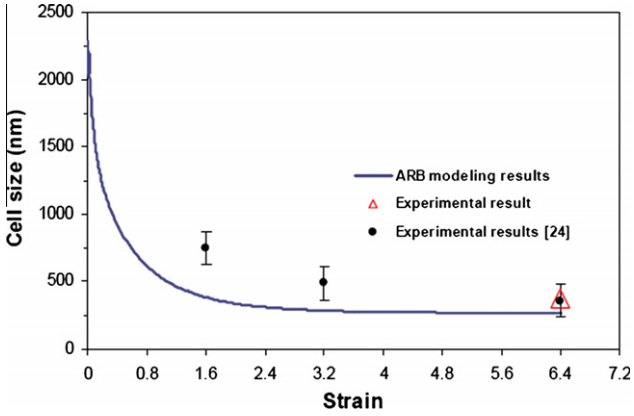

Fig. 6. Change of cell size as a function of accumulated strain.

to the parameters used in this study. Based on Fig. 6, it can be concluded that the dislocation-based model can predict the average grain size after each pass of ARB.

5. Conclusions

An existing two-phase composite model based on dislocation density evolution was used to predict the variation of yield strength and average grain size of AA1100 aluminum alloy during ARB passes. Comparison of the predictions with experimental results revealed that there is a good agreement between model predictions and experimental findings. Moreover, using this model some information about the hardening and recovery mechanisms can be obtained. Based on this model, it can be suggested that the hardening mechanism in the studied alloy is the increasing dislocation densities in both cell interiors and cell walls. Cross slip is the main recovery mechanism in cell interiors, while edge dislocation climb is responsible for recovery in cell walls. In summary, the variation of the yield strength and microstructure of AA1100 aluminum alloy by ARB passes can be predicted well by the use of a simple two-phase composite dislocation-based model.

References

[1] Valiev RZ, Islamgaliev RK, Alexandrov IV. Bulk nanostructured materials from severe plastic deformation. Prog Mater Sci 2000:103–89.
[2] Valiev RZ. Nanostructuring of metals by severe plastic deformation for advanced properties. Natur Mater 2004;3:511–6.
[3] Valiev RZ, Estrin Y, Horita Z, Langdon TG, Zehetbauer MJ, Zhu YT. Producing bulk ultrafine-grained materials by severe plastic deformation. JOM 2006;58:33–9.
[4] Saito Y, Utsunomiya H, Tsuji N, Sakai T. Novel ultra-high straining process for bulk materials development of the accumulative roll-bonding (ARB) process. Acta Mater 1999;47:579–83.
[5] Richert J, Richert M. A new method for unlimited deformation of metals and alloys. Aluminium 1986;62:604–7.
[6] Salishchev GA, Valiahmetov OR, Galeev RM. Formation of submicrocrystalline structure in titanium alloy VT8 and its influence on mechanical properties. J Mater Sci 1993;28:2898–902.
[7] Valiev RZ, Krasilinkov NA, Tsenev NK. Plastic deformation of alloys with submicron-grained structure. Mater Sci Eng A 1991;137:35–40.
[8] Horita Z, Smith DJ, Furukawa M, Nemoto M, Valiev RZ, Langdon TG. Evolution of grain boundary structure in submicrometer-grained Al–Mg alloy. Mater Charact 1996;35:285–94.
[9] Tsuji N, Saito Y, Lee SH, Minamino Y. ARB (accumulative roll-bonding) and other new techniques to produce bulk ultra fine grained materials. Adv Eng Mater 2003;5:338–44.
[10] Huang X, Tsuji N, Minamini Y, Hansen N. Characterization of ultra-fine microstructure in aluminum heavily deformed by accumulative roll-bonding (ARB). In: Proceeding of the 29th Riso international symposium on materials science, rosklide, Denmark: Riso national laboratory; 2001. p. 255–62.
[11] Belyakov A, Sakai T, Miura H, Tsuzaki K. Grain refinement in copper under large strain deformation. Phill Mag 2001;81:26–9.

[12] Lee SH, Saito Y, Tsuji N, Utsunomiya H, Sakai T. Role of shear strain in ultra grain refinement by accumulative roll-bonding (ARB) process. Scripta Mater 2002;46:281–5.
[13] Estrin Y, Toth LS, Molinari A, Brechet Y. A dislocation based model for all hardening stages in large strain deformation. Acta Mater 1998;46:5509–22.
[14] Toth LS, Molinari A, Estrin Y. Strain hardening at large strains as predicted by dislocation based polycrystal plasticity model. Eng Mater Technol 2002;124:71–7.
[15] Enikeev NA, Kimb HS, Alexandrov IV. Kinetic dislocation model of microstructure evolution during severe plastic deformation. Mater Sci Eng A 2007;460–461:619–23.
[16] Mckenzie PWJ, Lapovok R, Estrin Y. The influence of back pressure on ECAP processed AA6016: modeling and experiment. Acta Mater 2007;35:2985–93.
[17] Hosseini E, Kazeminezhad M. The effect of ECAP die shape on nanostructure of materials. Comput Mater Sci 2009;44:962–7.
[18] Hosseini E, Kazeminezhad M. A hybrid method on severe plastic deformation of copper. Comput Mater Sci 2009;44:1107–15.
[19] Hossini E, Kazeminezhad M. Dislocation structure and strength evolution of heavily deformed tantalum. Int J Refract Met Hard Mater 2009;27:605–10.
[20] Estrin Y, Molotnikov A, Davies CHJ, Lapovok R. Strain gradient plasticity modeling of high-pressure torsion. J Mech Phys Sol 2008;56:1186–202.
[21] Muller M, Zehetbauer M, Borbely A, Ungar T. Stage IV work hardening in cell forming materials, part I: features of the dislocation structure determined by x-ray line broadening. Scripta Mater 1996;35:1461–6.
[22] Pirgazi H, Akbarzadeh A, Petrov R, Kestens L. Microstructure evolution and mechanical properties of AA1100 aluminum sheet processed by accumulative roll-bonding. Mater Sci Eng A 2008;497:132–8.
[23] Winther G, Huang X, Godfery A, Hansen N. Critical comparison of dislocation boundary alignment studied by TEM and EBSD: technical issue and theoretical consequences. Acta Mater 2004;52:4437–46.
[24] Ezadjou M, Daneshmanesh H, Janghorban K. Microstructural and mechanical properties of ultra-fine grains (UFG) aluminum strips produced by ARB process. J Alloy Compd 2009;474:406–15.
[25] Baik SC, Estrin Y, Kim Hs, Helming RJ. Dislocation density based modeling of deformation behavior of aluminum under equal channel angular pressing. Mater Sci Eng A 2003;351:86–97.